ELSEVIER

Ceramics International 28 (2002) 791–803

CERAMICS INTERNATIONAL

www.elsevier.com/locate/ceramint

Sintering behaviour of Y_2O_3 powders prepared by the polymer complex solution method

P. Durán*, J. Tartaj, C. Moure

Instituto de Cerámica y Vidrio (CSIC), Electroceramics Department, 28500-Arganda del Rey, Madrid, Spain

Received 16 November 2001; received in revised form 12 December 2001; accepted 16 January 2002

Abstract

High purity fine Y_2O_3 powder has been prepared by a polymer complex solution method using polyethylene glycol as the complexant of Y^{3+} cations. Powder morphology and compacts prepared from three different powder characteristics have been studied. SEM observations were used to know the agglomeration degree of the powders, and the uniformity of powder compacts, and the Hg-porosimetry results to investigate the pore size and microstructure evolution during sintering of the green compacts. The compacts made with the powders calcined at the lower temperatures showed an almost single-peaked pore-size distribution and a more homogeneous microstructure, whereas the pore-size distributions of the compacts made with powders calcined at higher temperatures were double or triple peaked. The sintering behaviour of the low temperature calcined powders exhibited significantly better sinterability and higher densification rate/grain growth rate ratio than the high-temperature calcined powder compacts. Complex rearrangement phenomena relating the pore coordination numbers-grain size-grain morphology appear to occur in the initial and intermediate stages of sintering. In the final stage of sintering, grain growth modified the thermodynamic stability of remaining pores permitting its disappearance although kinetics impeded its complete elimination limiting, thus, the final density to values near theoretical density (≈99.5%).

Keywords: A. Sintering; D. Y_2O_3; Polymer solution

1. Introduction

Although the powder processing techniques for several oxide ceramics such as ZrO_2, TiO_2, Al_2O_3, etc. are well established and powders satisfying the necessary requirements for the fabrication of high-quality ceramics are now commercially available [1], it is not so in the case of Y_2O_3. This has a single oxidation state oxide over a wide temperature range, its structure is cubic up to about 2300 °C and transforms into a hexagonal structure at higher temperatures. These characteristics become such an oxide as a host material for scintillator used for nuclear medical imaging. Although fully dense Y_2O_3 is now commercially available it must be sintered at temperatures well above 1700 °C. Given that yttria transmits at longer IR wavelengths than most other oxides (9.5 μm cutoff) and, on the other hand, it has a superior thermal stability then this oxide becomes a good candidate for optical applications. However, this kind of material must be sintered to full density to avoid detrimental scattering at service conditions.

On the basis of the above mentioned characteristics, yttria could be a potential candidate for several applications, and the knowledge of those processing aspects leading to achieve fully dense materials becomes necessary. Rasmunssen et al. [2–4] studied the influence of several precipitation conditions on the sintering behaviour of Y_2O_3 and obtained a sintering density of about 95% of theoretical density at 1450 °C and about 99% at 1900 °C. Dogan et al. [5] investigated the influence of the precursor characteristics combined with freeze drying on the Y_2O_3 sintering behaviour. Green compacts containing monosized small pores could be sintered at 1250 °C to 95% and at 1450 °C to >99% of theoretical density. Ciftcioglu et al. [6] studied the effect of agglomerate strength on the sintering density of monosize spheres of agglomerated yttria powders compacts in air and under vacuum at 1400 °C. Densities no higher than about 94 and 98% of theoretical density, respectively, were achieved which were closely related to the

* Corresponding author. Tel.: +34-91-871-1800; fax: +34-91-870-0550.

E-mail address: pduran@icv.csic.es (P. Durán).

0272-8842/02/$22.00
PII: S0272-8842(02)00045-7

agglomerate strength distribution in the green compacts. The spherical yttria precursor had been obtained by dissolving urea in yttrium nitrate. In the same way, Sordelet and Akinc [7] studied the sintering of monosized and submicrometric spherical yttria powders in the 1500–1700 °C temperature range comparatively to a commercial raw Y_2O_3 powder. Although a higher sinterability was demonstrated for the monosized spherical Y_2O_3 powder, no fully dense ceramic bodies were achieved. Rhodes et al. [8] established the impurities levels tolerated for optical ceramics based on Y_2O_3 prepared from different powder precursors and sintered at 1700–2100 °C under vacuum and ranging from 93.8 to 99.9% theoretical density depending on the used precursor.

Presently, the sizes of commercially available powders are about 0.2–0.3 μm, but in the last decade many efforts are addressed to the use of finer powders in ceramic practices. The advantages of using powders of a size in the 10–20 nm range can lead to achieve dense bodies with a grain size in the nanoscale, i.e. less than 100 nm [9–11]. However, development in such an area needs the use of special methods for preparing and compacting powders which is a strong disadvantage for translating to a conventional ceramic processing. For example, nanophase metals and ceramic powders are now synthesized by evaporating the metal in an inert atmosphere and allowing it to condense on the surface of cold finger kept at the temperature of liquid nitrogen, with a final post-oxidation heat-treatment. On the basis of such a process, a variety of nanostructured metal-oxide ceramics such as ZrO_2, TiO_2, ZnO, MgO, and Al_2O_3 can be produced [12] but it is TiO_2 which is best characterized from its synthesis up to its microstructure, sintering, and mechanical properties [13–16]. An undesired feature of the inert gas condensation process is that the nanoparticles during the post-oxidation step, heat up to high temperatures for some seconds due to the exothermic nature of the oxidation and, as a consequence, some tendency to agglomeration is always present. By better controlling the oxidation step, Skandan et al. [17] obtained unagglomerated Y_2O_3 powders with an average particle size of 7 nm leading to green compacts with high transparency. More recently Chen and Chen [18,19] by a more conventional precipitation preparation method obtained almost fully dense Y_2O_3 ceramics at moderately low-temperatures (1200–1450 °C). As a consequence of their previous results, a two-stage sintering method without grain-growth for fully dense nanocrystalline doped-Y_2O_3 ceramics was proposed [20].

New approaches in the preparation of fine oxide powders are emerging in the last years [21–25]. These are based on the Pechini type process, i.e. the insitu polymerizable complex (IPC) method or another type of polymer complex solution (PCS) method which, in principle, could overcome some disadvantages of the IPC method. The IPC method has many advantages but with the disadvantage of the effective removal of large amounts of organic material. The PCS method is a simpler organic polymer gel one which differs from the IPC process in that utilizes water as a solvent instead of organic ones.

In the present work we prepared Y_2O_3 powders of high sinterability. In that way, reactive powders are thus essential for obtaining high-density Y_2O_3 ceramics. We have already prepared CeO_2 reactive powders from cerium nitrate and polyethylene glycol (PEG) by controlling the exothermal decomposition reaction. The easy compaction of the CeO_2 nanopowders and the high sinterability led to almost fully dense ceramics at relatively low temperatures (≈1250 °C). On that basis we prepared Y_2O_3 powder by the same polyethylene glycol-based process as well as the powder characteristics, and the sintering behaviour will be carried out.

2. Experimental procedure

Yttrium nitrate hexahydrate ($Y(NO_3)_3{\cdot}6H_2O$) was used as source of Y, and the details of the flow diagram for the Y_2O_3 powder preparation are given elsewhere [24]. Briefly, 0.1 mol of $Y(NO_3)_3{\cdot}6H_2O$ was dissolved into the minimal amount of water and added to an aqueous solution containing 0.1 mol of polyethyleneglycol $OH(–CH_2CH_2O–)_nH$ (PEG) with an averaged molecular weight of 200 with continuous stirring at about 90 °C for complete dissolution. After several hours of heating at 90 °C, a viscous organic gel without forming precipitation was produced. In order to obtain powder with different characteristics, the gel was calcined at 600, 725, or 800 °C for 1 h in static air in an electric furnace and hereinafter labeled as Y-1, Y-2, and Y-3 samples, respectively. In all cases the obtained Y_2O_3 powder was attrition milled with zirconia ball media for 4 h in methanol. After milling, the powders were characterized by X-ray diffraction with a diffractometer (Siemens D-5000, Erlangen, Germany). The crystallite size (D) of the nanosize powders was calculated using several diffraction lines from the Scherrer formula, $D = 0.9\lambda/\beta\cos\theta$, where λ is the wavelength of X-rays, β the corrected half-width that is obtained using the (111) line of the pure silicon as the standard. Specific surface areas of the differently calcined Y_2O_3 powders were measured by the single-point BET method (Quantachrome MS-16 model, Syosset, NY), using nitrogen as an absorbate after drying under vacuum. From the specific surface areas data, the particle sizes were also calculated using the equation, $\phi = 6/S\rho$, where ϕ is the average diameter of the assumed spherical particles, S the surface area of the powder, and ρ the theoretical density of Y_2O_3 (5.03 g/cm^3). The morphology of the Y_2O_3 powders was studied by SEM (Zeiss DSM 950, Oberkochem, Germany).

Ball milled and granulated powders were cold isopressed at 200 MPa. Pore size distributions of as pressed compacts were determined by mercury penetration porosimetry (Micromeritics, Autopore II, 9215, Norgross, USA). The samples were sintered in air using a dilatometer (Netzsch 402E of Geratebau, Bayern, Germany) at a heating rate of 5 °C/min. The isothermally sintered samples were heated in the temperature range of 1375–1440 °C for 0–10 h. Densities were measured by the Archimedes method in water.

The microstructure of sintered samples was examined by scanning electron microscope. The grain size was measured by the line intercept method on the polished and thermally etched sintered samples.

3. Experimental results

3.1. Powder characterization

Powder characteristics are listed in Table 1. The Y_2O_3 powders have a particle size ranging from 9 to 26 nm as measured by the X-ray line broadening, but they were constituted by soft and hard agglomerates ranging from 100 nm to 2 μm in all cases as observed by SEM and shown in Fig. 1. The surface area for Y-1 powder is larger (109 m^2/g) than for Y-2 and Y-3 powders (90 and 36 m^2/g) which contains both small and larger and dense agglomerates. However, the particle size calculated from the BET surface measurements was somewhat higher than that obtained by XRLB method indicating a certain agglomeration of the powders. Although the morphology of the powders is very similar, and the smaller agglomerates (≈150 nm in size) was present in all of them, but softer and looser agglomerates were in the case of the Y-1 and Y-2 samples.

3.2. Compaction behaviour

In spite of the different characteristics of the Y_2O_3 powders, the green density of the compacts was quite similar for the three Y_2O_3 green compacts. However, it must be mentioned that the powders with smaller particle size, i.e. the Y-1 sample showed a lower green density (41% theoretical density) than the others (42 and 46% theoretical density) for Y-2 and Y-3 samples, respectively.

Fig. 2 shows the pore-size distribution for green compacts of the three kind of Y_2O_3 powders. We can divide the pore size distribution in three well defined regions: (1) pores with size similar to the particle size or pores between the primary particles within an aggregate; (2) pores with size between 20 and 100 nm, i.e. pores between aggregates or intra-agglomerates pores (hereafter called first generation or matrix pores); and (3) pores with size higher than 100 nm or inter-agglomerate pores (hereafter called second generation pores). Comparing these results, it seems that those powders with the smaller particle size showed a more homogeneous pore size distribution, although the presence of a residual porosity with excessively large pores (>5 μm) was present in all the cases. Such porosity, as it is shown in Fig. 3, is caused by the presence of some strong agglomerates which do not fracture upon pressing.

3.3. Green compacts densification

Fig. 4 illustrates the shrinkage vs temperature data. According to Fig. 4(A), the samples Y-1 and Y-2 with a lower density initiate a detectable bulk shrinkage at a lower temperature (between 600 and 800 °C) than for the Y-3 sample with a higher green density, which initiates the shrinkage above 800 °C. Such behaviour can be connected with the different pore size of the green compacts. As it is shown in Fig. 4(B) some densification takes place in the Y-1 and Y-2 samples below 1000 °C while the densification starting is displaced up to 1200 °C in the case of the Y-3 sample. In all of them an end point density of 0.99 Dt was achieved at 1400 °C for the Y-1 sample and of 0.985 Dt at 1500 °C and 1600 °C for the samples Y-2 and Y-3, respectively.

Fig. 5 shows the densification rate vs sintering temperature for the different Y_2O_3 samples. It can be observed that the temperature for maximum densification rate increases with the inhomogeneity level, i.e. the higher temperature for maximum densification rate occurred in the Y-3 sample which contained a higher agglomeration degree. In this case two maxima at 1375 and 1440 °C were present which can be related with the elimination of smaller pores at the first maximum and the larger pores at the second one. Such a phenomenon, as shown in Fig. 4, delayed the end point density to a higher temperature. Comparing the temperatures and

Table 1
Main characteristics of Y_2O_3 calcined powders

Samples	Calcination temperature (°C)	Particle size (nm)			Surface area (m^2/g)
		XRLB	BET surface	SEM	
Y-1	650	9	11	≈100	109
Y-2	725	11	13	≈100	90
Y-3	800	26	33	≈150	36

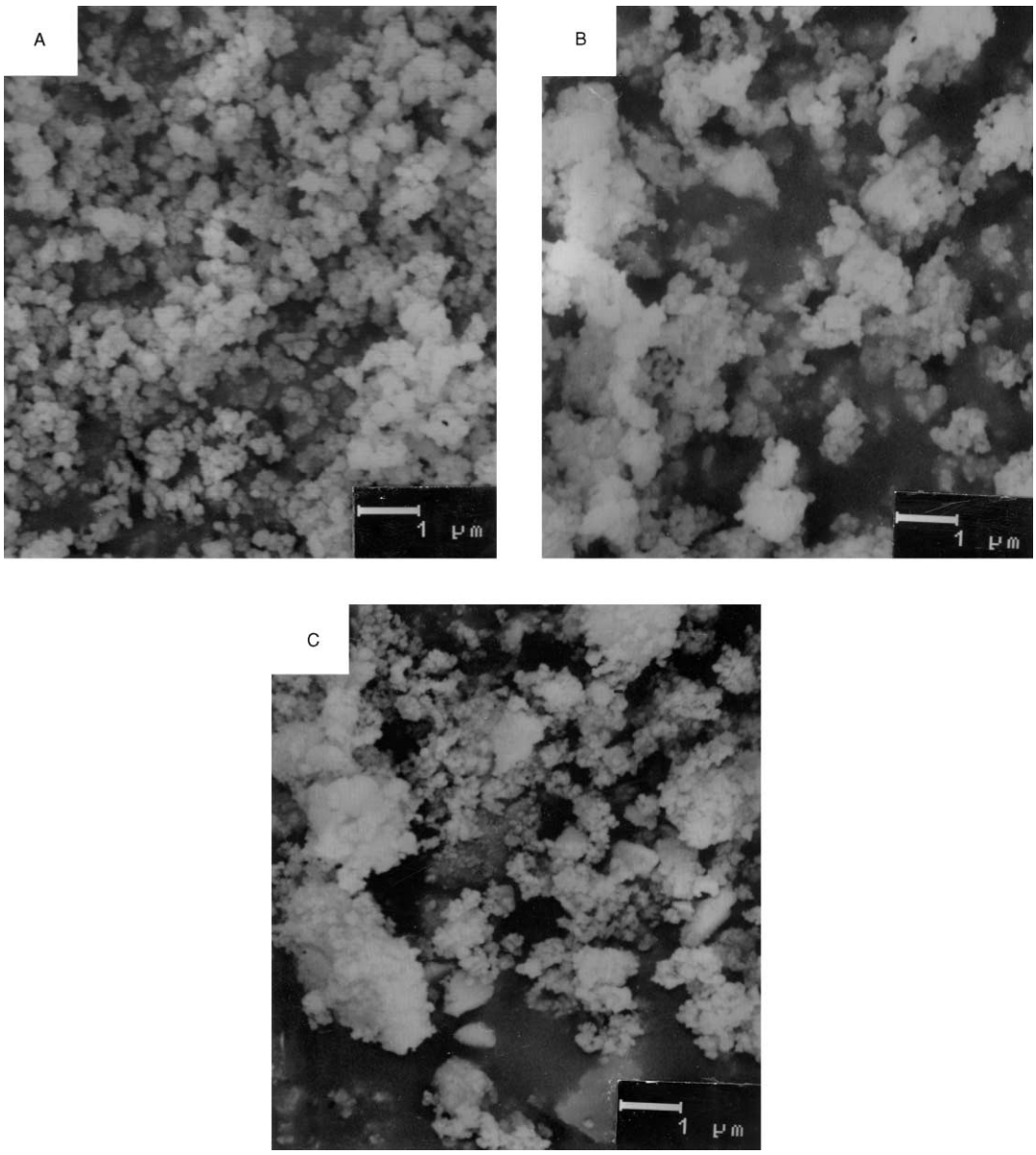

Fig. 1. SEM photomicrographs of the Y_2O_3 powders calcined at (A) 650 °C, (B) 725 °C, and (C) 800 °C.

densities of maximum densification rate, i.e. 1375 °C and 85% theoretical density for the Y-1 sample, 1410 °C and 70% theoretical density for Y-2 sample, and 1440 °C and 80% theoretical density for the Y-3 sample (second maximum), both temperature and the pore size distribution can be considered as the dominant factors for maximum densification rate because densities are quite different.

3.4. Sintering and microstructural evolution

The initial and intermediate stages of sintering have been studied by mercury porosimetry. The evolution of the pore size distributions as a function of sintering temperature for the three different Y_2O_3 powder compacts is shown in Fig. 6. As a common feature present in the three samples is that smaller pores disappear and larger ones growth and, as a consequence, the average pore size considerably increase. For example, in the case of the Y-1 sample, the average pore size increased from 22.6 nm in the green compacts to 31.5 at 700 °C, 41 nm at 800 °C, 89.5 nm at 1000 °C, and 137 nm at 1200 °C. On the other hand, Fig. 7 shows the change of total pore volume with sintering temperature. In the specific case of the Y-1 powder compacts, no perceptible change in the total pore volume is observed up to 600 °C. Above that temperature the total pore volume slowly decreased up to 1200 °C beyond which it decreased rapidly. Similar tendencies for the others two Y_2O_3 powders were found, but the temperatures for initial change in the total pore volume were displaced at 900 ° and 1100 °C for Y-2 and Y-3 samples, respectively.

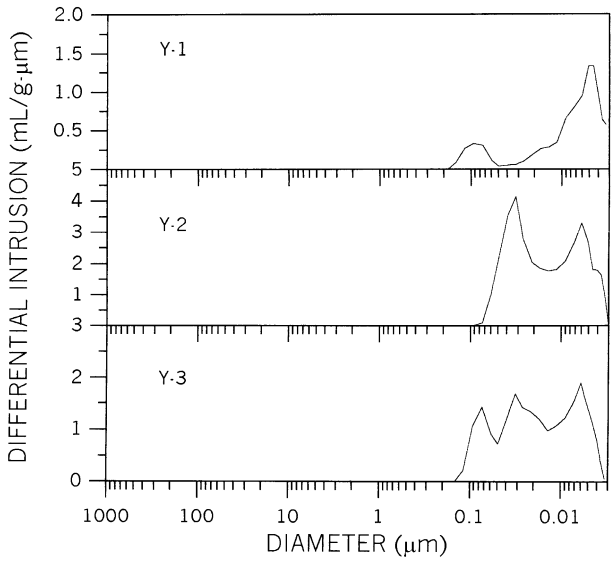

Fig. 2. Pore-size distribution of green compacts Y-1, Y-2, and Y-3 prepared by differently calcined Y_2O_3 powders.

Given that no appreciable densification (below 4%) took place up to the above mentioned temperatures, then it must be assumed that the disappearance of small pores takes place by surface diffusion [9]. If the total pore volume did not change in the corresponding temperature range for the different Y_2O_3 powders it must also be assumed some microstructural changes before starting the densification process, as for example a considerable growth of pores as previously stated.

Fig. 8, shows the microstructural evolution of the three Y_2O_3 samples sintered for 2 h in the temperature range of 800–1200 °C. For simplifying, the argumentation will be referred to the Y-1 sample being extensive to the Y-2 and Y-3 samples. In this case the initial particle size of the Y-1 powder was about 9 nm and the average pore size in the green compacts was of 22.6 nm. As the sintering temperature increases up to 700 °C the grain size increases up to about 100 nm, and the average pore size increases up to 31.6 nm. This indicates that the occurred grain growth led to certain pore coalescence and, simultaneously, to a better packing powder and lower pore coordination. At these conditions all those pores smaller than the critical pore coordination will

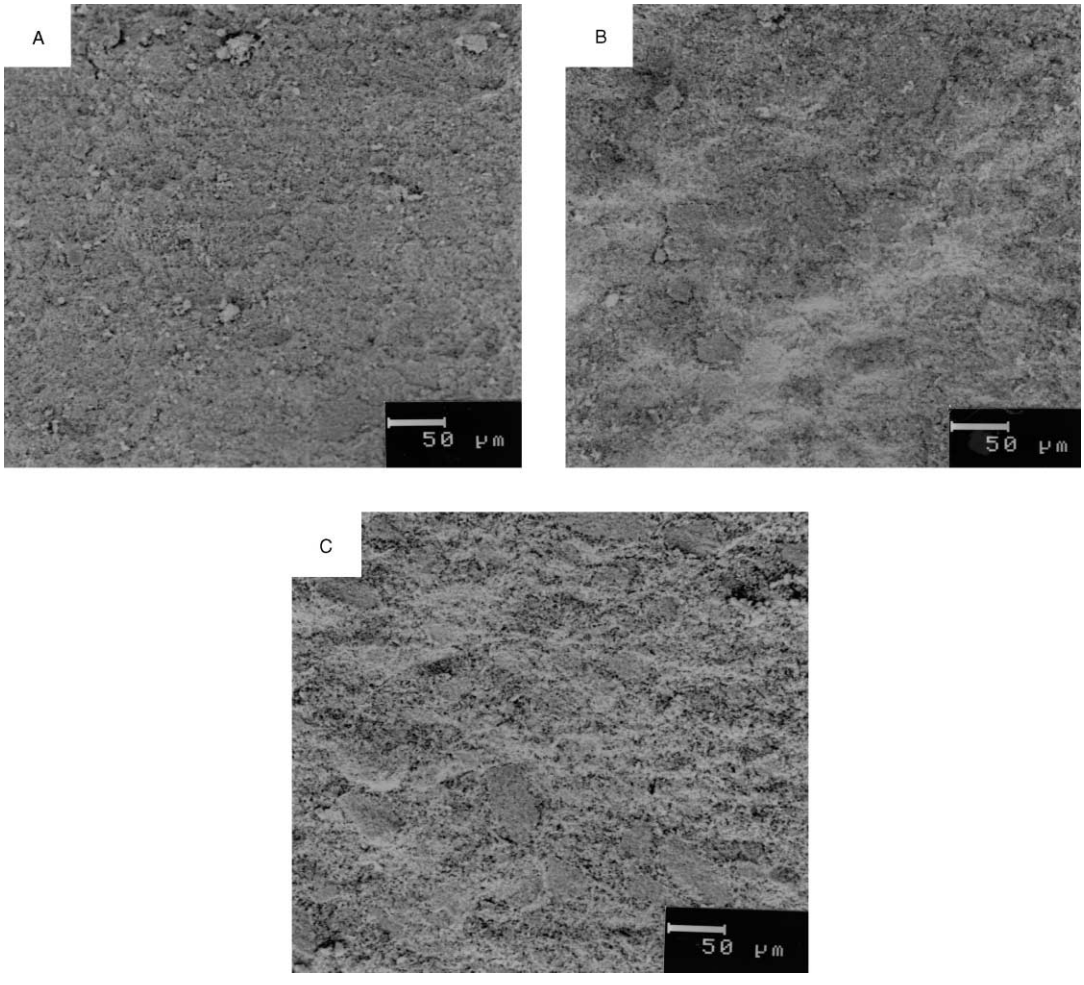

Fig. 3. Fracture surfaces of Y_2O_3 green compacts prepared by calcinations at (A) 650 °C, (B) 725 °C, and (C) 800 °C.

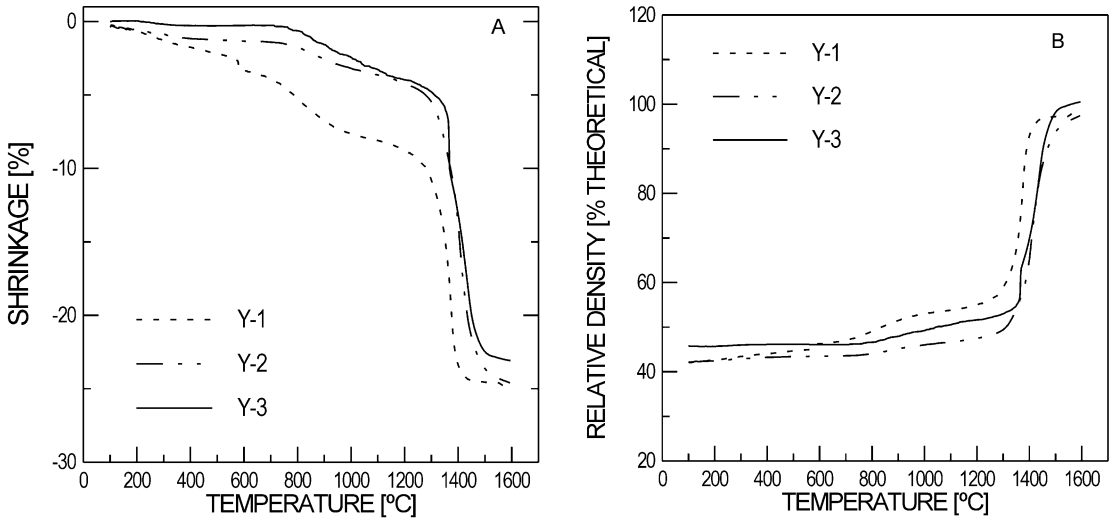

Fig. 4. Sintering behaviour of the different Y_2O_3 powders compacts: (A) shrinkage and (B) relative density versus sintering temperature.

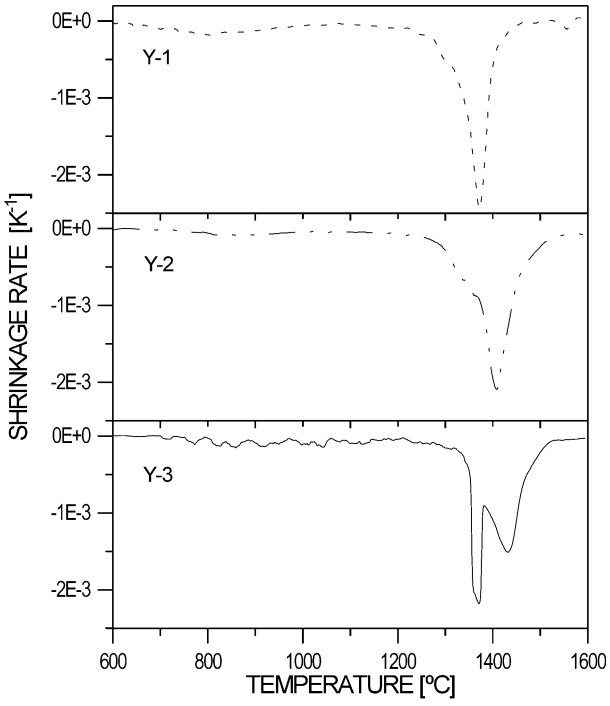

Fig. 5. Densification rate versus sintering temperature of compacts prepared by different Y_2O_3 powders.

have disappeared and the higher ones will grow [26]. For successively higher sintering temperatures the pore size/particle size ratio slowly shifted to values a little lower than the critical one and the sample slowly densifies. For temperatures higher than 1300 °C the pore size/grain size ratio is much more favorable than the critical, most of the porosity is eliminated and the sample strongly densifies. In a narrow temperature range (from 1300 to about 1400 °C) density changed from about 60 to 98% theoretical density. A transition from pores with convex surfaces to pores with concave ones was present, probably, near 1300 °C, and the majority of porosity is eliminated.

3.5. Densification and grain growth

Figs. 9 and 10 show the grain growth behaviour and density versus time for compacts of the different Y_2O_3 powders at the temperature for the higher densification rate, i.e. at 1375, 1400, and 1440 °C for Y-1, Y-2, and Y-3 samples, respectively. Grain growth kinetics adjusted quite well to a parabolic law of the type:

$$D^2 = A(T)t + K$$

where D is the grain diameter, $A(T)$ is temperature dependent, t is the time and K a constant. It is noticed that grain sizes progressed well in all of them beyond a critical grain size, and specially in the case of the Y-3 in which a relatively lower endpoint density was achieved. These results indicate that although the large pores become thermodynamically unstable permitting its disappearance, the presence of these in the final microstructures lead to assume that kinetics, rather than thermodynamics, is the predominant factor in the elimination of the large pores. By comparing the curves of Figs. 9 and 10 it is also noticed that in the case of the Y-1 sample, with a lower grain growth, the final sintered density was quite higher than in the case of the Y-3 sample. Such a finding confirmed the suggestions of Chao and Harmer [27] of enhanced final sintered density by inhibiting grain growth. Even so, the reached final end-point density for the Y-1 sample was only of 99% after firing for 10 h at 1375 °C, which indicates that some large pores being thermodynamically unstable, remained in the microstructure after a reasonable length of firing.

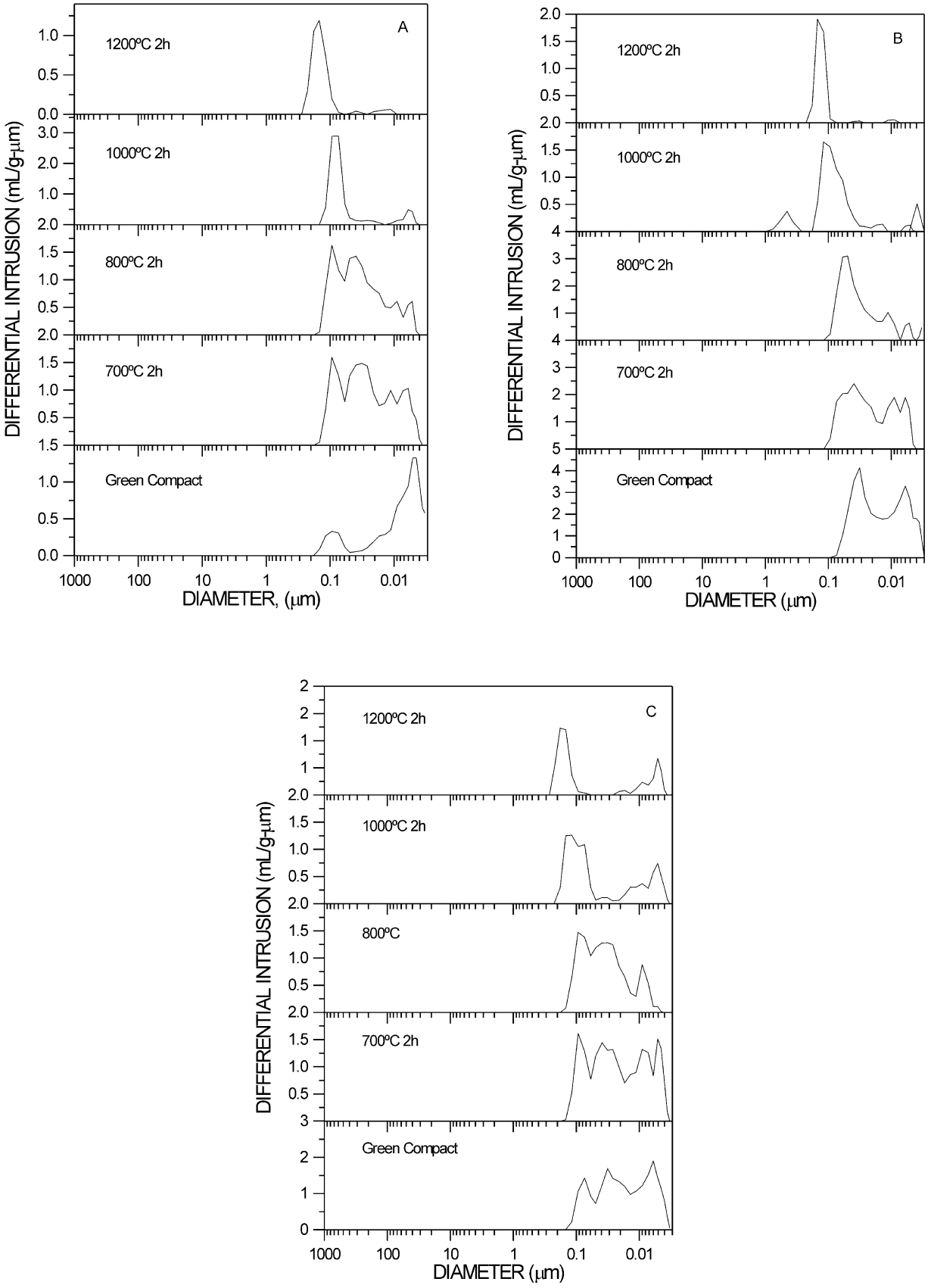

Fig. 6. Pore-size distribution versus sintering temperature of (A) Y-1, (B) Y-2, and (C) Y-3 powder compacts.

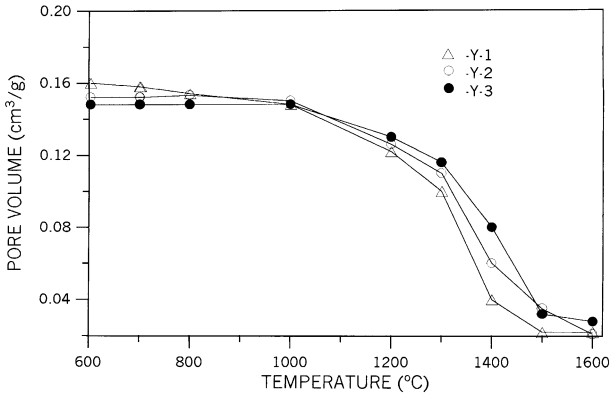

Fig. 7. Total pore volume versus sintering temperature of the different Y_2O_3 powder compacts.

Fig. 11 shows grain growth during sintering of Y_2O_3 samples by plotting the density against grain size. At temperatures near to 1400 °C the compacts of the Y-1 sample densifies at about 93.5% of the theoretical density with very little grain growth and the grain size remains within submicrometer range. At higher temperatures the densification rate is strongly reduced and simultaneously a significant grain coarsening takes place and the grain size increases to about 7.5 μm. It is interesting to note that beyond a given density (critical density?) a change in the trajectories is present. The steepleness of such a change may indicate if a determined sample would or would not be likely to densify completely after reasonable sintering times. A similar phenomenon ocurred for the Y-2 and Y-3 samples for

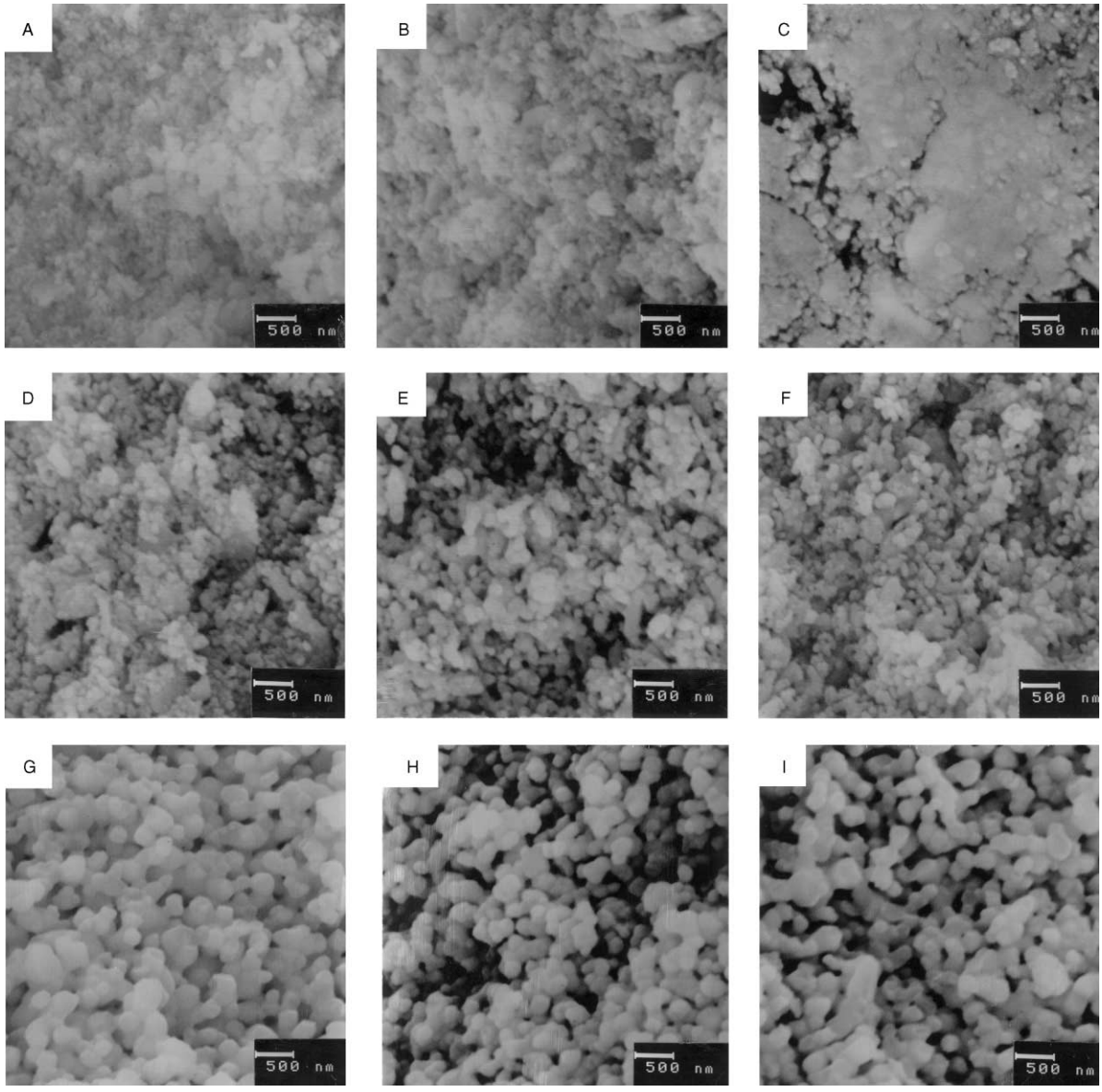

Fig. 8. SEM photomicrographs of fracture surfaces of Y-1, Y-2, and Y-3 samples sintered for 2 h at 800 °C (A–C), 1000 °C (D)(E)(F), and 1200 °C (G–I), respectively.

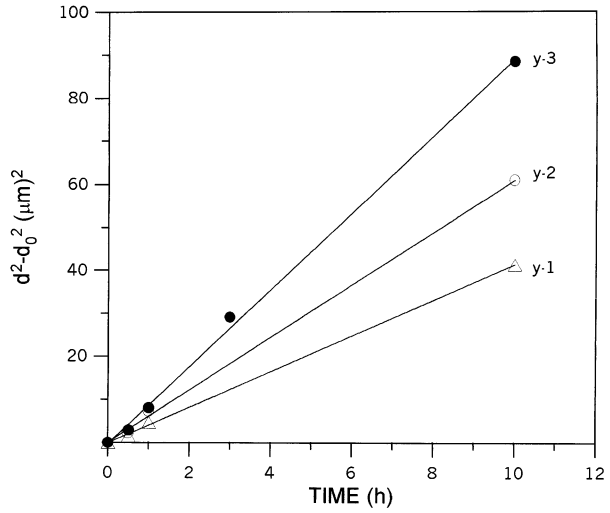

Fig. 9. Grain size of Y-1, Y-2, and Y-3 samples plotted as a function of sintering time at 1375, 1400, and 1440 °C, respectively. d_0 is the reference grain size at time t_0, and d is the average grain size at time t.

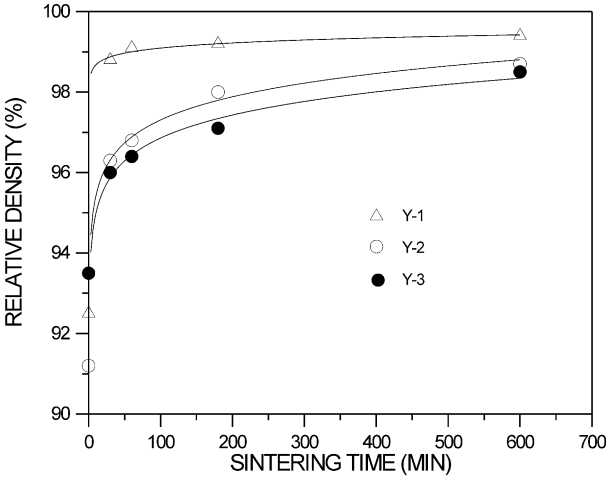

Fig. 10. Sintered density of Y-1, Y-2, and Y-3 samples as a function of firing time at 1375, 1400, and 1440 °C, respectively.

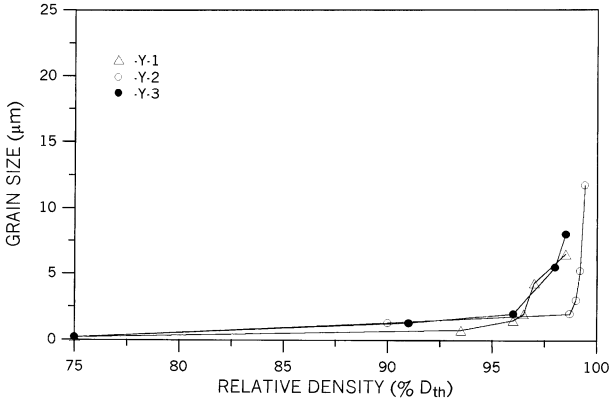

Fig. 11. Grain size versus density for the different Y_2O_3 sintered samples.

densities higher than 91 and 90% theoretical density, respectively.

Fig. 12 shows the microstructures of the different Y_2O_3 sintered samples after firing for 0, 3, and 10 h in the temperature range of 1375–1440 °C, i.e. at the intermediate sintering stage. In the microstructure of the sintered samples without isothermal held [Fig. 12(A), (D), and (G)] besides a detectable grain growth has taken place, the smaller pores have disappeared and the large pores grow, leading to a situation in which a mixture of pores with convex surface (minority interagglomerates porosity), and pores with concave surfaces in the almost fully dense regions are to exist. The fact that the larger pores (second generation) increases at this heat treatment can be due to pore coalescence. With increasing heat treatment simultaneously with the grain growth most of the pores in the Y_2O_3 matrix became larger, and an almost generalized shape change from convex to concave curvature took place [Fig. 12(B), (E) and (H)]. After a prolonged heat treatment period for 10 h [Fig. 12(C), (F), and (I)], most of the pores were coordinated by few grains and had concave surfaces. Some spherical pores were entrapped into larger grains. It must be mentioned that although the pores at this heat treatment are all thermodynamically unstable, the pores are not removed from the microstructure, i.e. there is a great difficulty in removing them kinetically. Ceramic bodies with a density higher than 99% of theoretical density were translucent.

4. Discussion

On the basis of the above results we must focus the discussion by assuming the following considerations: (1) the Y_2O_3 powders here studied are made by particles (mainly nanosized) with unequal size and irregular arrangements, as shown in Fig 1, (2) on compaction, the smaller (nanosized) particles pack together leading to the formation of dense agglomerates, surrounded by less dense regions (interagglomerates), (3) in powder compacts two types, at least, of pores exist. Those located between the nanosized particles, i.e. within the dense agglomerates, usually called as first-generation pores, and larger pores, i.e. those located between the agglomerates, which are called second-generation pores [27,28]. It must also be assumed that the pore coordination number of the first-generation pores will be much lower than the second-generation pores, and (4) on sintering such a powder compacts, simultaneous processes of densification and grain growth have to take place.

4.1. Packing arrangements and defects

The structure of Y_2O_3 green compacts is composed of dense regions (densified agglomerates) with a highly

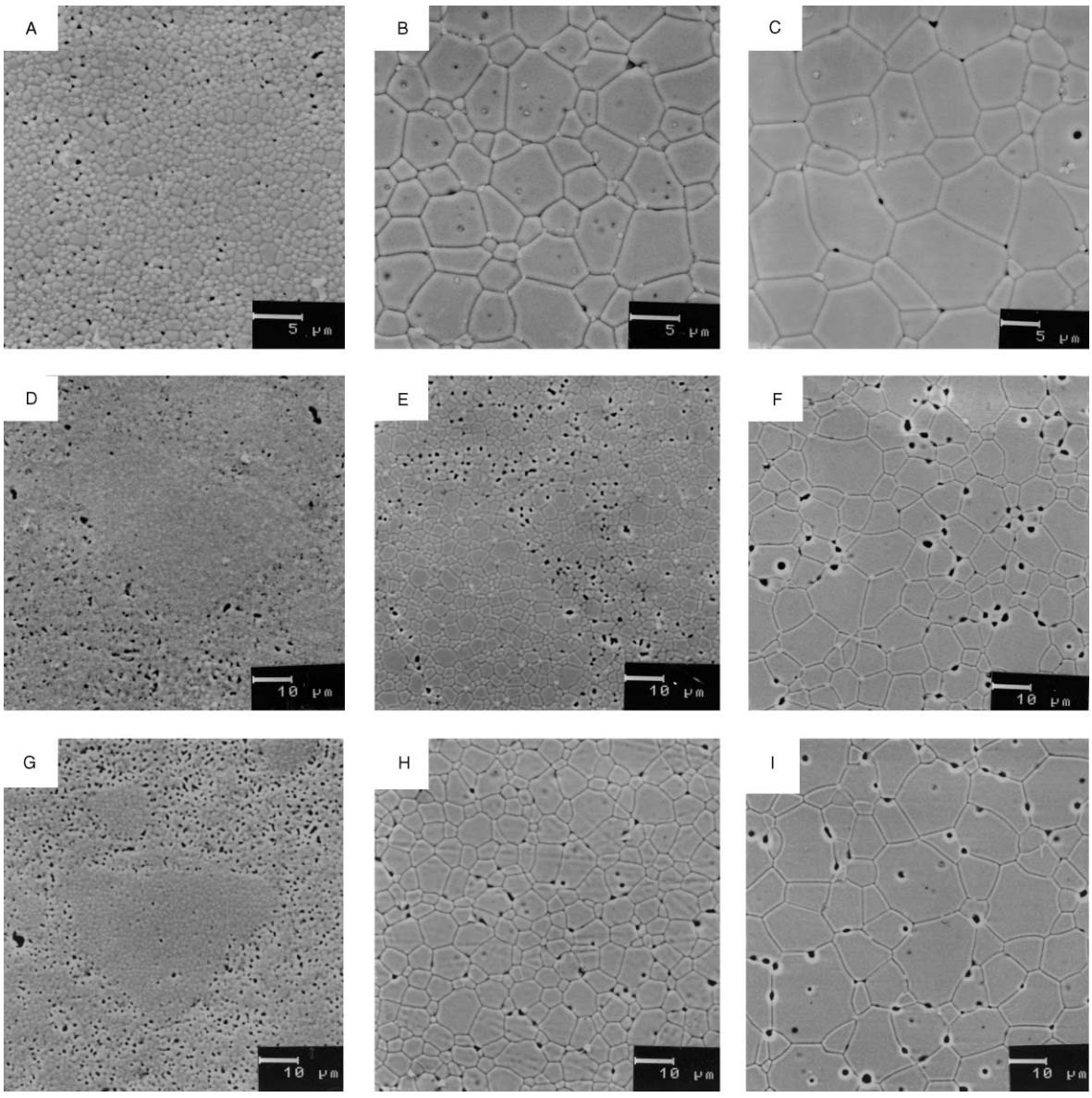

Fig. 12. Microstructural evolution as a function of sintering time for Y-1 samples (A–C), Y-2 samples (D–F), and Y-3 samples (G–I) at 1375, 1400, and 1440 °C, respectively.

ordered packing in whose interior are located all the smaller pores, i.e. those with a size equal or smaller than the particle size and, therefore, they are thermodynamically unstable as pointed out by Kingery and Francois [26]. The mentioned dense regions are apparently near free of defects, at least detectable by SEM, Fig. 3, although some small defects can exist due to small variations in particle size. The structure in the interagglomerate regions is quite disordered having arrays of particles with a coordination number higher than others and, therefore, pores with convex surfaces, i.e. with a coordination number much larger than the critical coordination number, are thermodynamically stable. As it is shown in Fig. 1, and clearer in Fig. 3, the structure of the interagglomerate regions is very heterogeneous with some inhomogeneities originated as consequence of non fractured agglomerates upon pressing.

4.2. Densification process

Although most of the known theories on the sintering of ceramic compacts into a dense body are based on approaches of spherical particles with a uniform size, shape, and stacking, it is clear from Figs. 4 and 5 that a close relation between the shrinkage rate and particle size, pore size, and grain growth has to exist. However, these parameters themselves individually cannot explain the relatively homogeneous final microstructure of the almost fully dense Y_2O_3 ceramic bodies (Fig. 12). In green compacts in which ceramic particles have different

individual coordination numbers, as it is the present case, a continuous internal collective reorganization of both pores and particles during sintering seems to occur. In that way, the Veringa model [29,30] can be applicable to our Y_2O_3 powder compacts. Such a model recognizes that a stacking of spherical particles having local variations in their individual coordination will exert a pressure on its immediate surroundings, depending such a pressure on both the total and local coordination. If somewhere in the stacking of particles a gradient exists in the local coordination, a force is acting on the particle considered into the direction of the area with highest coordination. Such a force generates a pressure that stimulates densification in zones with a relatively high density and causes dilution at places where the stacking density is lower than average. As pointed out by Sagel-Ranssijn et al. [31], this pressure will finally result in the formation or growth of flaws in the ceramics, and could explain the appearance of large defects after sintering in agglomerated green compacts, which already presented small defects in the green compacts.

Taking into account the results shown in Fig. 4(B) a lower green density was found for the samples with finer particles, but due to the larger driving force and the shorter diffusion distances the densification rate at the early stages of sintering is higher (Fig. 5). For example, in the case of the Y-1 samples the relative density increases by about 18% (i.e. from 41 to 59% theoretical density), while the Y-3 samples increases by only 7% (i.e. from 46 to 53% theoretical density). The Y-2 sample has an intermediate behaviour and the green density increases by about 10% (i.e. from 42 to 52% theoretical density). A simultaneous evolution of the total pore volume with increasing temperature occurred with a decrease in the case of the Y-1 samples and apparently without change in the other two Y-2 and Y-3 samples. In all of them a disappearance of the smaller pores and the appearance of larger pores took place. Although the enhancement of the densification rate for Y-1 samples could be explained by a higher particle packing and a smaller average pore size, the global phenomena occurring in the early stages of sintering can be associated with the concept of critical pore coordination number, and assuming a certain flexibility for the ceramic matrix.

At first, it must be assumed for simplicity a mixture of two kind of pores in our Y_2O_3 green compacts, those with a size smaller than the particle size and, therefore, can be considered thermodynamically unstable, and those larger than the particle size and are thermodynamically stable. At the early stages of sintering the smaller pores mainly located within agglomerates will be rapidly eliminated and de agglomerates, mainly composed of primary particles, will densify. In that way, the Y-1 and Y-2 samples will have the higher densification rate (Fig. 5). The Y-3 sample, with an average pore size higher than the particle size will need higher temperatures to eliminate the pores and, effectively, the total pore volume of such a sample does not shift up to or above 1000 °C, while in the case of the Y-1 and Y-2 samples a total pore volume decreasing was already present from 600 and 800 °C, respectively (Fig. 7). Two simultaneous processes could be envisioned at these early stages of sintering: (1) elimination of pores with a coordination number smaller than the critical value, as proposed by Kingery and Francois [26], and (2) a certain grain growth process is initiated. These two processes have hardly been initiated in the Y-3 samples and its densification is lower. Although some little amount of pores smaller than the critical value have been eliminated, but the majority of them, having a coordination numbers higher than the critical value, remain thermodynamically stable. With the densification and grain growth above that temperature, the coordination number of the larger pores decrease, the pore size/particle size ratio will be below the critical value and the larger pores, now thermodynamically unstable, could be removed. As it is shown in Fig. 8, the grain size increased at 1000 °C up to about 200 nm in the Y-3 sample and up to 150 nm in the Y-1 and Y-2 samples, and the average pore size was about 100 nm in all the cases. The pore size/grain size ratio is well below the thermodynamic critical value, the pores start to be eliminated and the Y_2O_3 green compacts rapidly densifies [Fig. 4(B)]. However, as it is shown in Fig. 4(B), a densification level of 90% theoretical density, i.e. near the end of the intermediate sintering stage, was achieved for the Y-1 sample at a temperature 100 °C lower than for the other two Y_2O_3 samples. In the final sintering stage, although almost all pores are thermodynamically unstable, some of them are not eliminated at the higher temperature limiting, thus, the achieved final density was below the theoretical. A similar phenomenon was observed by Zhao and Harmer [27] at the final stage of sintering of alumina even in the most ideal grain growth conditions because of kinetics, rather than thermodynamics is the determining factor.

4.3. Microstructure homogenisation

As pointed out by Gupta [32] grain growth occurred through all stages of sintering and, as it is shown in Fig. 8, once necks form grain growth proceeded in a generalized manner in the sample as the temperature and time increased. Grain growth firstly starts in the denser regions (agglomerates) at the same time that the inter-agglomerates void decreases its coordination number. Given that voids can pin the grain coarsening process, the grain size in the inter-agglomerates regions will be slightly smaller than within agglomerates. There is a competition between these two processes. In the measure that some of the pores with coordination number lower than the critical one are eliminated the particle packing increases and the grain growth process

will be favored. When the pore size is the same in both agglomerates and inter-agglomerates regions the grain growth process will be uniform and the grain size will be homogenized with sintering time, despite the vast difference in the green microstructure. This statement is consistent with theoretical predictions of Thomson et al. [33] and Chen and Chen [19] for isotropic grain growth, which is similar to the present case for Y_2O_3 with cubic structure (Fig. 9).

As observed in Fig. 11 linear relations seems to exist between grain size and density at densities up to 93.5% theoretical density for the Y-1 sample, 91% theoretical density for the Y-2 sample, and 90% theoretical density for the Y-3 sample. These results supported the contentions that pore elimination and grain growth simultaneously occurred and, probably, both processes takes place by the same mechanism as suggested by Gupta [32] and Coble [34]. These differences in the grain growth behavior can be attributed to differences in the initial packing uniformity in the green compacts (see Fig. 3). Although the presence of regions denser than others was a common fact in the different Y_2O_3 compacts, the more uniformly packed Y-1 samples developed few dense sintering regions and, therefore, the grain size did not increase until densities higher than 93.5%. On the contrary, the presence of many local areas consisting of fine particles in the Y-3 sample will gives rise to a rapid densification and, thus, grains would grow from a lower sintering temperature. As shown in Fig. 12 different regions of the sample undergo different grain growth rates and, therefore, a broader grain size distribution was found. Quite similar results were found by Merkert et al. [35] on sintering of agglomerated nanocrystalline (25 nm) Y_2O_3. They suggested that a homogeneous green body should be used for reducing the coarsening rate in the initial and intermediate stages of sintering.

5. Conclusions

1. Ultra-fine powders of Y_2O_3 with high sinterability have been obtained using a polyethilenglycol-based process, i.e. the PEG method.
2. Sinterability of Y_2O_3 powders was found to be sensitive to the calcination temperature, particle size, and pore size distribution of the green compacts.
3. Although the pore size evolution showed similar trends for the differently calcined powders, a higher pore growth degree was observed for the more nonuniform powder compacts in the early sintering stages.
4. During sintering of these agglomerates-containing green compacts many simultaneous phenomena take place with the disappearance of pores (those with coordination number lower than the critical), growth and/or shrinkage of those pores with coordination number higher than the critical, and some grain growth at the lower temperature.
5. On raising temperature agglomerates sinter faster than the inter-agglomerates regions as a consequence of both a higher packing density and smaller pore size and, depending on the densification rate in those regions, it may or may not take the place in formation of fissures. If this is so, then a new rearrangement process at higher temperatures increasing the number of contacts can help to close such fissures.
6. In those green compacts with narrower pore-size distribution the grain growth process seems to be ralentized up to a density higher than in the compacts with a wider pore-size distribution. As consequence of this, a higher densification rate/grain growth rate ratio was also shown, at least until almost the end of the intermediate stage of sintering. However such a behaviour led to the closure of some pores that, being in the growth rather than the shrinkage regime, stopped further densification. Such a behavior indicated that the grain size plays an important role on the kinetics of small and large-pore removal.
7. Fine and translucent ceramics of Y_2O_3 (>99% theoretical density) with a grain size less than 1 μm below 1400 °C can be easily prepared by the PEG method.

Acknowledgements

The present work was supported by the Spanish CICYT under contract MAT-2000–815

References

[1] H. Hahn, Microstructure and properties of nanostructured oxides, Nanostruct. Mater. 2 (1993) 251–265.
[2] M.D. Rasmussen, G.W. Jordan, M. Akinc, O. Hunter, M.F. Berard, Influence of precipitation procedure on sinterability of Y_2O_3 prepared from hydroxide precursor, Ceram. Int. 9 (2) (1983) 59–60.
[3] M.D. Rasmussen, M. Akinc, M.F. Berard, Effect of precursor freeze-drying conditions on sinterability of hydroxide-derived Y_2O_3 powders, Ceram. Int. 10 (3) (1984) 99–104.
[4] M.D. Rasmussen, M. Akinc, O. Hunter Jr., Processing yttria powders derived from hydroxide precursor, Ceram. Int. 11 (2) (1985) 51–55.
[5] F. Dogan, A. Roosen, H. Hausner, Influence of hydroxide precursor processing on the densification of yttrium oxide powders, in: G.L. Messing et al. (Eds.), Advances in Ceramics, Vol. 4, Ceramic Powder Science, The Am. Ceram. Soc., Westerville, OH, 1986, p. 681.
[6] M. Ciftcioglu, M. Akinc, L. Burkhart, Effect of agglomerate strength on sintered density for yttria powders containing

agglomerates of monosize spheres, J. Am. Ceram. Soc. 40 (11) (1987) C329–C334.
[7] D.J. Sordelet, M. Akinc, Sintering of monosized spherical yttria powders, J. Am. Ceram. Soc. 71 (12) (1998) 1148–1155.
[8] W.H. Rhodes, E.A. Tricket, D.J. Sordelet, Key powder characteristics in sintered optical ceramics, in: G.L. Messing, S. Hirano, H. Hausner (Eds.), Ceramic Powder Science, II, The Am. Ceram. Soc. Inc, Westerville, OH, 1990, p. 677.
[9] H. Hahn, J. Logas, R.S. Averback, Sintering of nanocrystalline TiO_2, J. Mater. Res. 5 (3) (1990) 609–614.
[10] M.J. Mayo, D.C. Haghe, D.J. Chen, Processing nanocrystalline ceramics for applications in superplasticity, Mater. Sci. Eng. A166 (1993) 145–159.
[11] R.S. Averback, H.J. Hofler, R. Tao, Processing of nano-grain materials, Mater. Sci. Eng. A166 (1993) 169–177.
[12] P.K. Kumar, K. Keizer, A.J. Burggraaf, T. Okubo, H. Nagamoto, S. Morooka, Densification of nanostructure titania assisted by a phase transformation, Nature 358 (1992) 48–51.
[13] H. Hahn, J. Logas, R.S. Averback, Sintering characteristics of nanocrystalline TiO_2, J. Mater. Res. 5 (1990) 609–614.
[14] M. Ghernazi, P. Pirouz, H.J. Hofler, H. Hahn, R.S. Averback, Temperature dependence of the harness of nanocrystalline titanium dioxide, J. Am. Ceram. Soc. 74 (10) (1991) 2672–2674.
[15] R. Birringer, H. Gleiter, H.P. Klein, P. Narquardt, Nanocrystalline materials: an approach to a novel solid structure with gas-like disorder, Phys. Lett. A. 102 (1984) 365–369.
[16] R.S. Averback, H. Hahn, H.J. Hofler, J. Logas, T.C. Shen, Kinetic and thermodynamic properties of nanocrystalline materials, Mater. Res. Soc. Symp. Proc. 153 (1989) 3–12.
[17] G. Skandan, H. Hahn, J.C. Parker, Nanostructured Y_2O_3: synthesis and relation to microstructure and properties, Scripta Metall. Mater. 25 (1991) 2389–2393.
[18] P.L. Chen, I.W. Chen, Reactive cerium (IV) oxide powders by the homogeneous precipitation method, J. Am. Ceram. Soc. 76 (6) (1993) 1577–1583.
[19] P.L. Chen, I.W. Chen, Sintering of fine oxide powders: I, Microstructural evolution, J. Am. Ceram. Soc. 79 (12) (1996) 3129–3141.
[20] I.W. Chen, X.H. Wang, Sintering dense nanocrystalline ceramics without final-stage grain growth, Nature 404 (2000) 168–171.
[21] M.P. Pechini, Method of preparing lead and alkaline earth titanates and niobates and coating methods using the same to form a capacitor. US Patent No. 3.330.697, 11 July 11.
[22] M. Kakihana, M. Yoshimura, Synthesis and characteristics of complex multicomponent oxides prepared by polymer complex method, Bull. Chem. Soc. Jpn. 72 (1999) 1427–1443.
[23] S. Yamamoto, M. Kakihana, S. Kato, A polymer complex solution route to the low temperature synthesis of tetragonal ZrO_2–CeO_2 with reduced amount of organic substance, J. Alloys Compos. 297 (2000) 81–86.
[24] P. Duran, F. Capel, D. Gutierrez, J. Tartaj, C. Moure, Cerium (IV) oxide synthesis and sinterable powders prepared by the polymeric organic complex solution method, J. Eur. Ceram. Soc., 22 (9–10) (2002) 1711–1721.
[25] P. Duran, F. Capel, J. Tartaj, C. Moure, Sintering behaviour and electrical properties of nanosized doped-ZnO powders produced by metal-organic polymer processing, J. Am. Ceram. Soc. 84 (8) (2001) 661–668.
[26] W.D. Kingery, B. Francois, The sintering of crystalline oxides: I, Interactions between grain boundaries and pores, in: G.C. Knezynski, N.A. Hooton, C.F. Gibbon (Eds.), Sintering and Related Phenomena, Gordon and Breach, New York, 1967, pp. 23–34.
[27] J. Zhao, M.P. Harmer, Effect of pore distribution on microstructure development: II, First- and second-generation pores, J. Am. Ceram. Soc. 71 (7) (1988) 530–539.
[28] F.F. Lange, Sinterability of agglomerated powders, J. Am. Ceram. Soc. 67 (2) (1984) 83–89.
[29] H.J. Veringa, Sintering models and the development of instabilities, J. Mater. Sci. 26 (1991) 5985–5995.
[30] H.J. Veringa, Statistical treatment of the sintering model and ceramic morphology development, J. Mater. Sci. 28 (1993) 2757–2762.
[31] C.D. Sagel-Ranssijn, A.J.A. Winnubst, B. Kerkwijk, A.J. Burggraaf, H. Verweij, Production of defect-poor nanostructured ceramics of yttria-zirconia, J. Eur. Ceram. Soc. 17 (1997) 831–841.
[32] T.K. Gupta, Possible correlation between density and grain size during sintering, J. Am. Ceram. Soc. 55 (5) (1972) 276–277.
[33] C.V. Thomson, H.J. Frost, I. Spaepen, The relative rates of secondary and normal grain growth, Acta Metall. 35 (4) (1987) 887–890.
[34] R.L. Coble, Sintering of crystalline solids: II, J. Appl. Phys. 32 (5) (1961) 793–799.
[35] P. Merkert, H. Hahn, J. Rödel, Sintering behaviour of nanocrystalline Y_2O_3, Nanostruct. Mater. 12 (1999) 701–704.